

Efficient Oxygen Evolution Reaction Catalyzed by Ni/NiO Nanoparticles Produced by Pulsed Laser Ablation in Liquid Environment

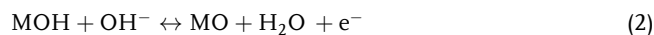
Valentina Iacono,* Salvatore Mirabella,* and Francesco Ruffino

Electrochemical water-splitting, sustained by renewable energy, is aimed at green H₂ production. Efficient and sustainable electrocatalysts are required for a proper energy transition. Oxygen evolution reaction (OER) in alkaline electrolyte can be pursued by using earth-abundant elements-based catalysts, such as Ni oxyhydroxides. A proper optimization of intrinsic properties and synthesis procedure is still needed. Herein, the synthesis of Ni/NiO nanoparticles (NPs) through a physical and green technique, pulsed laser ablation in liquid (PLAL), is presented. Ablating a Ni target in deionized water, at different ablation times, leads to NP dispersions used for realization of OER electrode onto graphene paper. Ion-beam analysis of catalysts amount and homogeneity of NP-based electrode is performed for the electrode optimization in terms of electrochemical performances. An overpotential at 10 mA cm⁻² of 306 mV is achieved for 40 μg cm⁻² of catalyst, while lowering the catalyst amount to 8 μg cm⁻², unprecedented turnover frequency of 0.20 s⁻¹ and mass activity of ≈1.3 A mg⁻¹ are reached. These data show that Ni/NiO NPs produced by PLAL are highly effective for OER in alkaline media and encourage the use of PLAL as a green and efficient technique for electrocatalyst production.

1. Introduction

Conventional fossil fuels are no longer sustainable for a sustainable development of our society. As a result, the majority of countries are eager to develop an alternative supply of renewable energy.^[1] Among the possible strategies, Hydrogen has many favorable features such as efficiency, zero emissions, and renewability.^[2] Electrochemical water-splitting is one of the most studied methods for the production of highly pure H₂ on short time and with a restricted impact on the environment.^[3–5] Indeed, supplying the electrochemical water-splitting with renewable energy would guarantee the production of green hydrogen. To efficiently split water, the two half reactions, the hydrogen evolution reaction (HER) and the oxygen evolution reaction (OER), should be assisted with highly active electrocatalysts. Recently, water electrolyzers in alkaline media attract the interest of scientific community for promising and sustainable performances, allowing the scalable production of low-cost hydrogen from renewable sources.^[6] In this scenario, the OER is a limiting reaction, involving the transfer of four electrons through reactions at high barriers. One of the most famous mechanisms is Krasil'shchikov's Path. In alkaline media, it is described by Equations (1)–(3), where M denotes surface-active sites^[7,8]

community for promising and sustainable performances, allowing the scalable production of low-cost hydrogen from renewable sources.^[6] In this scenario, the OER is a limiting reaction, involving the transfer of four electrons through reactions at high barriers. One of the most famous mechanisms is Krasil'shchikov's Path. In alkaline media, it is described by Equations (1)–(3), where M denotes surface-active sites^[7,8]




The mostly active materials for OER, Ir₂O₃ and RuO₂, are still not sustainable being too rare and costly.^[9,10] Thus, great attention has been aimed on the use of not-critical materials, such as Ni (hydro) oxide and Fe (hydro) oxide, which reduces the cost of the entire device giving a significant stability and catalytic activity in alkaline electrolyte.^[5,11–13]

In the framework of sustainable economy and pollution, reducing disposal and contaminants coming from the final product of a synthesis route has to be taken in consideration. Unfortunately, the mostly used synthesis techniques for oxides

V. Iacono, S. Mirabella, F. Ruffino
Dipartimento di Fisica e Astronomia “Ettore Majorana”
University of Catania
Via S. Sofia 64, 95123 Catania, Italy
E-mail: valentina.iacono@dfa.unict.it; salvo.mirabella@dfa.unict.it

V. Iacono, S. Mirabella, F. Ruffino
CNR-IMM (Consiglio Nazionale delle Ricerche - Istituto per la microelettronica e microsistemi)
Catania University
Via S. Sofia 64, 95123 Catania, Italy

F. Ruffino
Research Unit of the University of Catania
National Interuniversity Consortium of Materials Science and Technology (INSTM-UdR of Catania)
Viale Andrea Doria 8 and Via S. Sofia 64, 95125 Catania, Italy

 The ORCID identification number(s) for the author(s) of this article can be found under <https://doi.org/10.1002/pssb.202200590>.

© 2023 The Authors. physica status solidi (b) basic solid state physics published by Wiley-VCH GmbH. This is an open access article under the terms of the Creative Commons Attribution-NonCommercial License, which permits use, distribution and reproduction in any medium, provided the original work is properly cited and is not used for commercial purposes.

DOI: 10.1002/pssb.202200590

are chemical based and mostly require vacuum systems or high temperature and pressure.^[14]

Pulsed laser ablation in liquid (PLAL) is a physical technique that allows the production of pure and ligand-free nanoparticles (NPs) focusing a high-power pulsed laser beam focused on a solid target immersed in a liquid. PLAL doesn't need pressure or high-temperature systems because the interaction between the laser and the target generated itself a high temperature and pressures self-confined in the limited space coincident with the laser spot. Also, no pollutant waste is generated in obtaining the final product, making this technique "green".^[14] PLAL is an easy-to-use and quite versatile technique; in fact, varying the liquid environment in which the ablation takes place, different material composition could be obtained. Hence, ablating a metallic target in oxygen-rich liquid environment, such as deionized water, metal-oxide nanostructures could be synthesized. PLAL has been recently considered as a green synthesis technique of nanomaterials which have been exploited in hydrogen storage, production, and sensing.^[15] Recently, laser-based production of metal oxides NSs for water-splitting application has been reported.^[16–18]

In particular, among transition metal-oxide nanomaterials, nickel oxide has generally achieved lots of interest due its properties such as catalysis, energy storage, magnetism, optics, antibacterial activity, gas sensing, and biosensing.^[19–24]

Nickel-based NSs have been synthesized via laser ablation in liquids ablating nickel target in different liquids, such as water. The laser-based synthesis of Ni-based nanostructures for water-splitting has been recently reported. In particular, the synthesis is usually combined with electrophoretic deposition as an easy OER-electrode preparation method.^[17,18] Unfortunately, the OER performance obtained are not quite competitive in terms of extrinsic parameters (i.e., overpotential) and low attention has been devoted to the intrinsic activity of the electrocatalyst.

Here, in this article, we present the synthesis of Ni/NiO NPs obtained ablating a nickel target in deionized water with a nanosecond pulsed laser at different ablation time (5, 10, and 20 min). The as-synthesized NPs are transferred onto graphene paper (GP) varying the deposition technique, that is, drop casting and spin coating, and the amount of NPs dispersion. Rutherford backscattering spectrometry (RBS) measurement is employed for analyzing the homogeneity of the NPs distribution and the catalyst amount measurement. We observed that the spin-coating results in a better homogeneity. Thus, the OER activity is studied for the samples loaded with Ni/NiO NPs obtained at different ablation time. An overpotential at 10 mA cm⁻² of 306 mV was achieved for 40 μg cm⁻² of catalyst, while lowering the catalyst amount to 8 μg cm⁻², a turnover frequency (TOF) of 0.20 s⁻¹ and mass activity of ≈1.3 A mg⁻¹ were reached.

2. Experimental Section

2.1. Synthesis of the Ni/NiO NPs

A pulsed (10 ns) Nd:Yttrium Aluminum Garnet Laser (Quanta-ray PRO-Series pulsed Nd:YAG laser), operating at wavelength of 1064 nm, mean output power 5 W, and repetition rate of 10 Hz, was used to ablate a nickel target (purity 99.99%, diameter 25 mm, thickness 0.1 mm) in deionized water (resistivity 18 MΩ cm).^[25]

The nickel target was placed at the bottom of a Teflon cylindrical vessel and mersed with 8 mL liquid (**Figure 1a**).

The laser beam was focused with a lens (focal length 10 cm) and the laser fluence per pulse was 10 J cm⁻². Ni/NiO NPs were produced at different ablation time (*t*: 2, 5, 10, and 20 min). The Ni target was weighted before and after the ablation to extract the amount of Ni ablated for each synthesis performed. For this measurement, a microanalytical balance (Sartorius M5) with a sensitivity of 100 μg was used. Thus, the ablated mass derived for each synthesis was an experimental error of 0.2 mg. The obtained NP dispersion was stored at 4 °C for the stability of the solution and avoided NPs agglomeration.

2.2. NPs Characterization

Surface morphology of the NPs was analyzed by using a scanning electron microscope (SEM, Gemini field-emission SEM Carl Zeiss SUPRA 25, FEG-SEM, Carl Zeiss Microscopy GmbH, Jena, Germany).

The nanostructures' crystalline structure was analyzed by X-ray diffraction (XRD) technique. The sample for this analysis was realized by drop casting 0.5 mL of NP dispersion (at *t* = 5 min) onto Corning glass and drying in ambient condition. The XRD measurement was done in grazing incidence mode ($\theta_{\text{inc}} = 0.2^\circ$) using a Smartlab Rigaku diffractometer, equipped with a rotating anode of CuK α radiation ($\lambda = 1.54184 \text{ \AA}$) operating at 45 kV and 200 mA.

To realize the electrode, the NPs were dropped onto GP substrate. The amount of catalyst loaded and its homogeneity over electrode was evaluated by RBS (2.0 MeV He⁺ beam at normal incidence) with a 165° backscattering angle by using a 3.5 MV HVEE Singletron accelerator system (High Voltage Engineering Europa, Netherlands). RBS spectra were analyzed by using XRump software.^[26] From the RBS analysis, the atomic density (at cm⁻²) of the catalyst (Ni) was extracted integrating the Ni RBS signal peak. The resolution of the spectrometry was given by Poisson statistics. This allowed the evaluation of the error in the dose determination by considering $1/\sqrt{N}$, with *N* number of events (counts). The dose obtained allowed us to quantify the catalyst mass, or catalyst loading, in milligrams considering the molar mass of Nickel.

2.3. Electrode Realization

After the NPs synthesis, the NP dispersion was casted onto GP substrate (1 × 1.5 cm², 240 μm thick, Sigma Aldrich, St. Louis, MO, USA) first rinsed with deionized water and dried in N₂ to clean its surface. The catalyst loading mass and deposition techniques were varied to study the effects on electrochemical performance during OER in alkaline media. The amount of NP dispersion in one drop was fixed at 20 μL. Two different deposition techniques were used: the drop casting and the spin coating.

We named electrodes with the number of drops and the deposition technique (e.g., NiO_{3D} refers to the electrode realized by drop casting (D) 3 drops of the NP dispersion on the GP, while NiO_{3S} referred to 3 drops spin coated (S) on GP). In summary, four electrodes were realized as reported in **Table 1**. All the electrodes were characterized after drying the dispersion casted on the GP using a hot plate at 80 °C for 1 h.

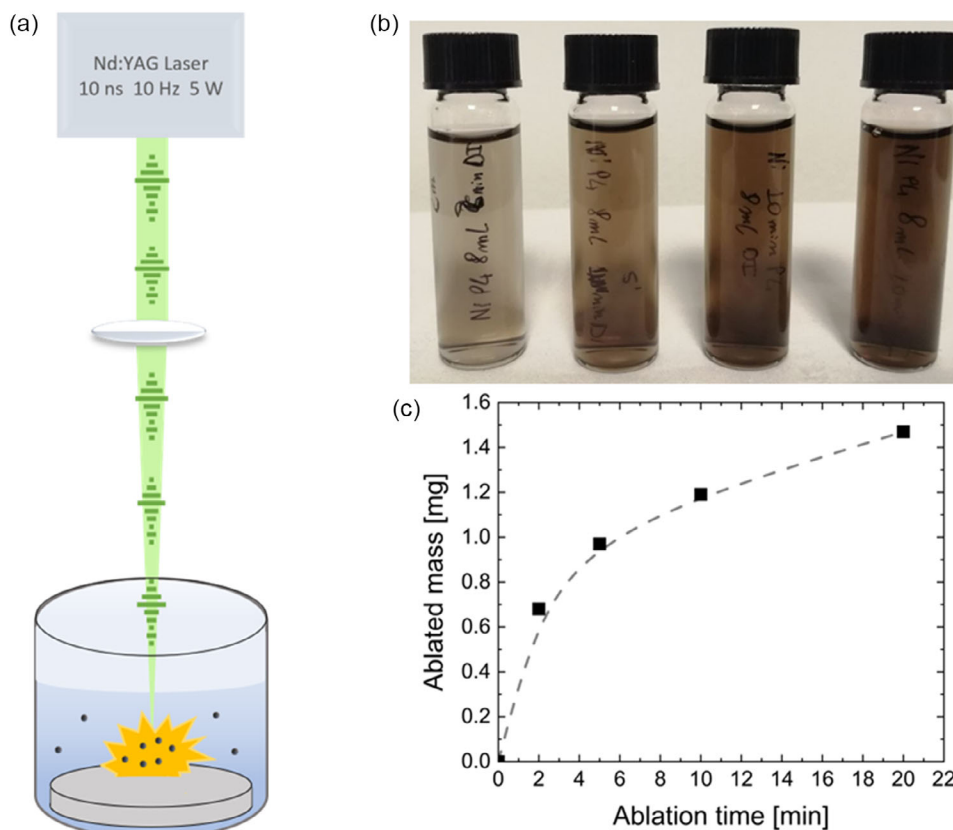


Figure 1. a) Schematic of pulsed laser ablation in liquid (PLAL) setup. b) From the left, nanoparticle (NP) dispersion obtained at 2, 5, 10, and 20 min of ablation. c) Mass of Ni target ablated varying the ablation time.

Table 1. Electrode preparation.

Sample	NiO _{3D}	NiO _{5D}	NiO _{3S}	NiO _{5S}
Amount of dispersion [μ L]	60	100	60	100
Deposition technique	Drop casting	Drop casting	Spin coating	Spin coating

2.4. Electrochemical Analysis

All the electrochemical measurements were performed at room temperature and atmospheric pressure. Electrochemical analyses were performed using a Versastat-4 potentiostat in a three-electrode setup using 40 mL of 1 M KOH (pH = 14) as the supporting electrolyte. A Pt wire was used as the cathode, a saturated calomel electrode (SCE) as the reference electrode and the GP with the Ni/NiO NPs as working electrode. Each electrode was stabilized performing a cyclic voltammetry (CV) at a scan rate of 10 mV s⁻¹ in the potential range 0–0.7 V versus SCE. Then, linear sweep voltammetry (LSV) at scan rate of 5 mV s⁻¹ in the same potential windows was done. The LSV curves report the potential in the x -axis versus RHE obtained

$$E_{\text{RHE}} = E_{\text{SCE}} + 0.242 + 0.059 \text{ pH} \quad [\text{V}] \quad (4)$$

From the LSV data, the overpotential (η) versus RHE was derived. For the comparison among the different electrodes, the η at

10 mA cm⁻² was considered. Electrochemical impedance spectroscopy (EIS) was performed with a superimposed 10 mV sinusoidal voltage in the frequency range 10⁴ ÷ 10⁻¹ Hz at a potential just after the onset potential (the minimum potential at which a reaction product is formed at an electrode).

The extracted uncompensated resistance (R_u) was used for the iR drop determination. The potential of the polarization curves obtained from the LSV measurements was corrected with the iR (i is the current) as follows

$$E_{\text{RHE } iR \text{ drop free}} = E_{\text{RHE}} - iR_u \quad [\text{V}] \quad (5)$$

Then, the Tafel slopes were derived reporting the overpotential as a function of the log of the current density. After the extrinsic OER activity determination, the intrinsic catalytic activity of the PLAL–electrocatalysts was studied calculating the TOF and the mass activity. TOF expressed the rate of production of oxygen molecules per active site. Among the approach reported in literature, we evaluated TOF as follows^[27]

$$\text{TOF} = \frac{i}{4nF} \quad [\text{s}^{-1}] \quad (6)$$

where i is the measured current at a fixed overpotential, 4 are the electrons involved in the OER, F is the Faraday constant, and n is the number of moles of the active sites. Mass activity was calculated dividing the current density 10 mA cm⁻² by the catalyst

mass. The catalyst mass and the number of moles were derived from the Ni dose value obtained through the RBS measurements. Chronoamperometry analysis was employed to study the stability of the PLAL-based electrode in a 1 M KOH electrolyte for 12 h at a constant current density of 10 mA cm^{-2} .

3. Results and Discussion

3.1. Ni/NiO NPs: Synthesis and Characterization

Figure 1a shows the schematic of PLAL process used for the synthesis of Ni/NiO NPs. The laser beam ($\lambda = 1064 \text{ nm}$) is focused by the lens onto the Ni bulk target immersed in 8 mL deionized water. Due to the interaction of the laser beam with the target, in few hundreds of picoseconds, a plasma plume is made up. A mechanical shockwave is then released as the plasma rapidly grows and led to a vapor phase called cavitation bubble containing vaporized liquid and ablated material. Temperature and pressure conditions are out of physical equilibrium allowing the definition of the chemical composition and structure of nanostructures. Depending on pulse energy and pulse duration, the bubble collapses after hundreds of microseconds releasing NPs in the liquid.^[14,28] For each synthesis, we kept constant the liquid volume and the laser fluence.

The laser fluence was estimated by dividing the mean output power of the laser, 5 W, by the laser spot area on the target in a pulse measured with SEM.^[28] We varied the ablation time from 2 to 20 min. Hence, we obtained 4 NP dispersions.

Regarding the structural properties of the NPs, we report in Figure S1, Supporting Information the XRD pattern characterizing the 5 min obtained dispersion dropped onto corning glass. The XRD pattern shows the peaks referred to the cubic Ni and the cubic NiO. The two peaks, two dominant peaks at 2θ values of 44.60° and 51.98° , refer to Ni (111) and Ni (200) while those at 37.33° and 43.38° correspond to NiO (111) and NiO (200). No structural changes were seen in the other samples obtained at a different ablation time. As expected, NiO presence is due to the oxidation of Ni NPs because the ablation occurs in oxygen-rich environment.^[29–32]

Figure 1b shows the solution's color became browner increasing the ablation time. This is related to an increase in the concentration of NPs in the colloid as the time for which the synthesis occurs increases.^[28] For a proof of concept, we weighted the Ni target before and after each synthesis. As Figure 1c shows, increasing the ablation time, a higher amount of Ni target is ablated. The trend of the ablated mass increasing the ablation time is not linear. The incremental ratio seems to decrease at higher values of time, maybe due to some laser-scattering effects from the ongoing formed NPs in solution, hence reducing the ablation rate.^[31,33] The ablation time is considered a key parameter for the productivity of the PLAL technique, indeed.^[28]

3.2. Electrode Preparation

After the synthesis, the best procedure for electrode preparation, in terms of the approach to transfer the NPs from the solution to the substrate, was investigated. We fix the attention on the NP dispersion at $t = 5 \text{ min}$ trying to obtain the highest homogeneity

as possible. We compared the uniformity of the NPs distribution onto GP using drop casting or spin coating, 3 or 5 drops. The drop area of the GP substrate was 1 cm^2 .

RBS analysis (spot area of 1 mm^2) was carried out in some points of the electrode to study the homogeneity of the NPs distribution and to derive the Ni dose for each electrode (Figure 2).

As reported in Figure 2a, the RBS measurement was done in four different spots of the dropped area to check the Ni amount distribution. Figure 2b shows the RBS spectrum centered in the Ni backscattering energy region: the signal at energy of 1.53 MeV refers to He^+ ion backscattered from Ni present at the sample surface, while data at lower energy refer to backscattering events occurring below the surface. The plot reports the RBS of NiO_{3S} , NiO_{5S} , NiO_{3D} , and NiO_{5D} samples. Integrating the Ni RBS peak, the Ni amount can be obtained within an experimental error of 1–2%. The values of the Ni dose are listed in Table 2.

The RBS curves of Figure 2b reflect a difference in the amount of Ni dropped in each sample. The 5-drops samples contain almost two times more material compared to 3-drops samples. Ni peaks profile of the drop-casted samples appears larger indicating a thicker NPs film.

Regarding the Ni distribution over the drop area, Figure 2c shows the values of Ni dose in four different points of each sample. The obtained Ni dose values for the main points analyzed were used to extract a mean value and a standard deviation (σ^2). As reported in Figure 2c, the drop-casted samples show higher values of σ^2 compared to the spin-coated ones, as expected.

To better detail the homogeneity of NiO_{3S} , we performed RBS measurements in eight different points of the electrode surface.

To test if any difference in NP dispersion solution occurs by varying ablation time, we prepared few electrodes with NP dispersion solutions obtained at the three-ablation time (5, 10, and 20 min). Given the previous results, we spin-coated 3 drops of dispersion (NiO_{3S} samples), Figure 3a,b compares the plan-view SEM images for $t = 10$ and 20 min. The Ni/NiO NPs are organized in a uniform and dense film covering the substrate containing spherical NPs.

The NPs size ranges approximately around 10 nm of diameter. From the SEM images, the 20 min sample seems to contain more material than the 10 min, as expected.

We have already observed, in Figure 1c, that the amount of Ni ablated in 20 min is higher compared to the 10 min. Figure 3c reports single-spot RBS measurements, confident of the uniformity of the NPs distribution on the electrode surface as discussed previously.

The Ni dose obtained for the three electrodes are listed in Table 3. Analyzing the RBS peaks, the Ni peak for the NiO_{3S} 20 min is the largest, pointing out the thickest Ni NPs film. As Figure S2, Supporting Information, shows, this is also reflected on the Oxygen peaks' profile. The Ni and O peaks of the 5 and 10 min samples are thinner compared to the 20 min. Basing on the thickness of the NiO_{3S} 5 and 10 min, we estimate an average thickness of about 20 nm while the thickness of the Ni NPs in the 20 min results about 90 nm.^[34] This could be associated to the higher concentration of the solution which, for the same volume of NP dispersion, results in a denser NPs-drop area. Also, the NiO_{3S} 20 min RBS profile has a

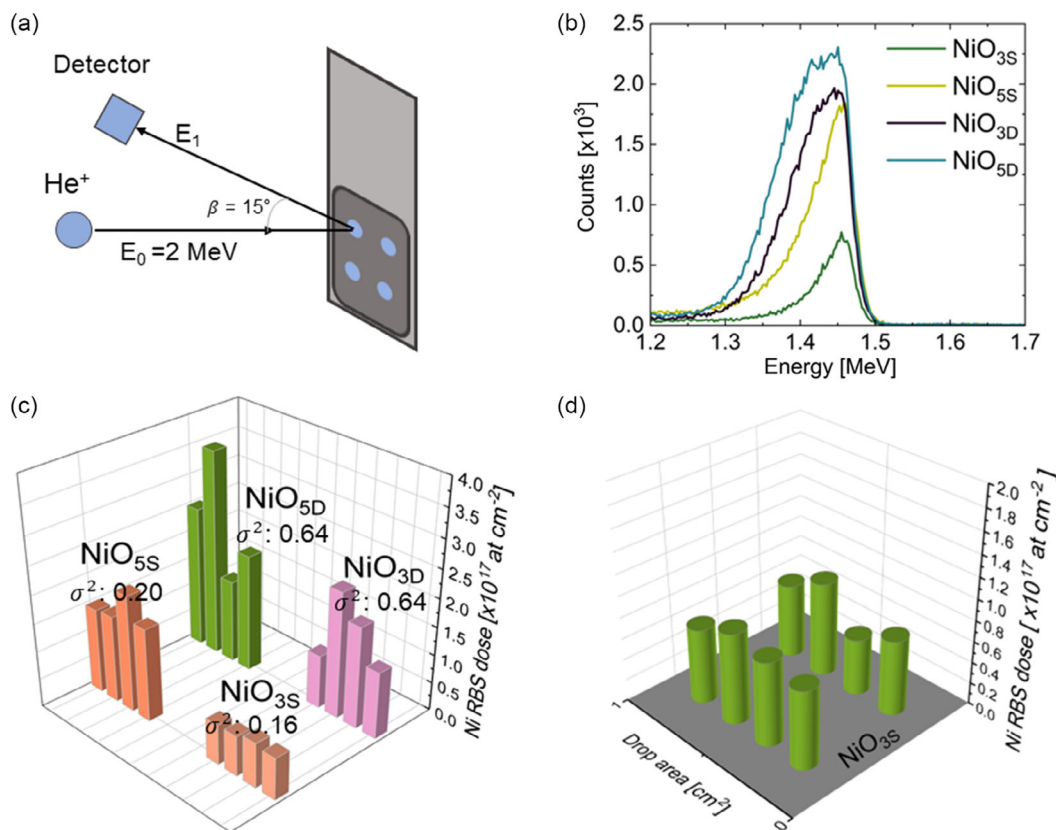


Figure 2. a) Schematic of the Rutherford backscattering spectrometry (RBS) measurement on the drop area (dark box, 1 cm^2) of graphene paper (GP) substrate (grey box). The incident 2 MeV He^+ -ion beam has a spot area of 1 mm^2 (blue spots). b) RBS plot for each electrode showing Ni peaks. c) The 3D bar plot showing the RBS Ni dose (proportional to the Ni peak area) measured in four different spots for each electrode. d) The 3D bar plot showing the map of RBS Ni dose for the $\text{NiO}_{3\text{S}}$ electrode in eight different points of the dropped area.

Table 2. RBS-extracted values of Ni dose for the $\text{NiO}_{3\text{S}}$, $\text{NiO}_{5\text{S}}$, $\text{NiO}_{3\text{D}}$, and $\text{NiO}_{5\text{D}}$ electrodes.

Sample	RBS Ni dose [$10^{17} \text{ at cm}^{-2}$]
$\text{NiO}_{3\text{S}}$	0.79
$\text{NiO}_{5\text{S}}$	1.51
$\text{NiO}_{3\text{D}}$	1.61
$\text{NiO}_{5\text{D}}$	2.46

pronounced left-hand asymmetry for the Ni and O peaks. This is typically observed with the increase of the roughness of the film analyzed.^[35] This asymmetry could be slightly noted also for the RBS spectra shown in Figure 2b. However, this could be useful for the comparison of the electrodes obtained using the same volume of colloid related to the different ablation time.

3.3. OER Activity with the Variation of Ablation Time

The electrochemical measurements were performed in 1.0 M KOH.

In the discussion, we will focus the attention on the electrochemical results obtained for those electrodes realized with the NPs

obtained at different ablation time. The electrochemical outcomes for the electrodes used for testing the optimization of the electrode preparation are discussed in the Supporting Information. Table S1, Supporting Information, lists all the data regarding the extrinsic OER parameters from the electrochemical analysis.

After performing 40 CV cycles in the range 0–0.7 V for the stabilization of the electrode, the LSV measurement was done. Figure 4a shows the LSV curves. The potential is reported versus RHE and 100% corrected with the iR drop value. The uncompensated resistance, R_u , was extracted fitting the EIS curves obtained just after the onset potential.^[36,37]

Figure 4b collects the EIS curves obtained for each tested electrode. Comparing the three electrodes LSV, the $\text{NiO}_{3\text{S}}$ 20 min results with the best performance.

The overpotential at 10 mA cm^{-2} of the $\text{NiO}_{3\text{S}}$ 20 min electrode is 306 mV. This low overpotential for the electrode containing the highest value of catalyst ($38.8 \mu\text{g}$) could be associated to the higher availability of catalyst sites for the OER activity. Also, the roughness deductible from the RBS spectra and the SEM image has ensured a good homogeneity of the NPs film providing more accessible Ni sites for the OER reaction. Indeed, the overpotential is considered an extrinsic parameter for the OER activity and it is well reported the decrease of the overpotential increasing the catalyst

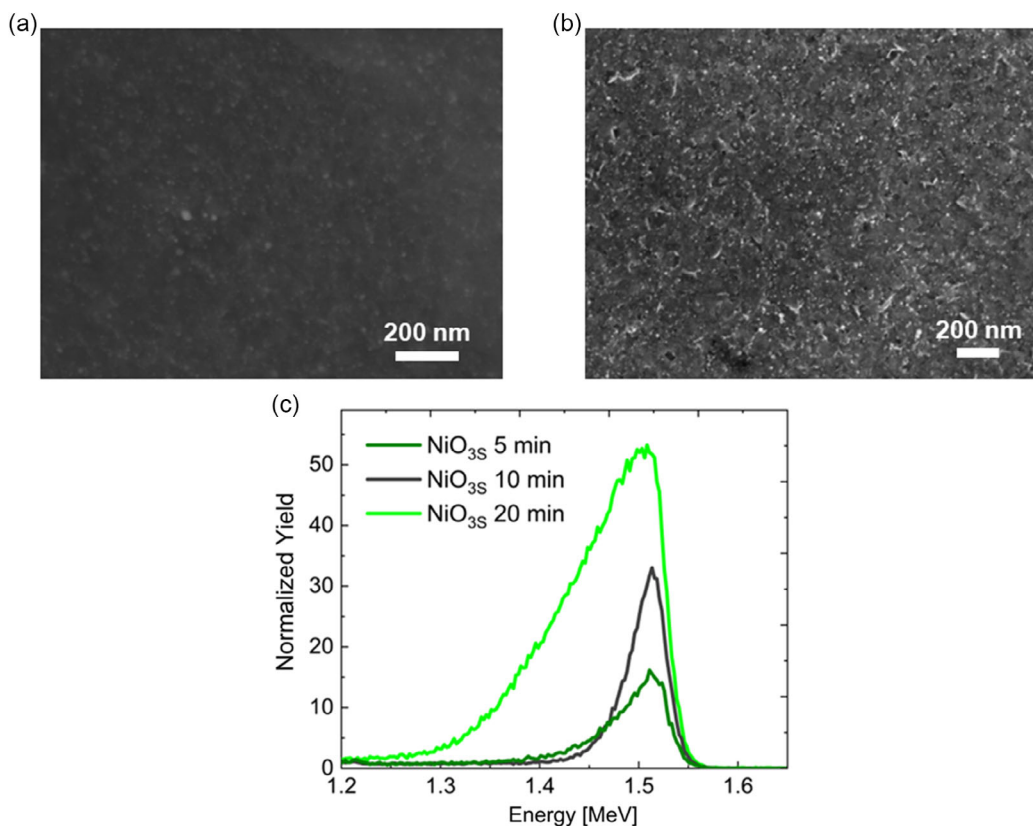


Figure 3. a) Scanning electron microscope (SEM) plan view of the NiO_{3S} 10 min electrode. b) SEM plan view of the NiO_{3S} 20 min electrode. c) Mean RBS Ni dose obtained for NiO_{3S} at the $t = 5, 10, 20$ min.

Table 3. OER intrinsic parameters obtained in 1 M KOH electrolyte. TOF and mass activity are evaluated at 10 mA cm⁻².

Electrode	η versus RHE @ 10 mA cm ⁻² [mV]	Tafel slope [mV dec ⁻¹]	Dose Ni [10 ¹⁷ at cm ⁻²]	Catalyst loading [μ g]	TOF [s ⁻¹]	Mass activity [A mg ⁻¹]
NiO _{3S} 5 min	337	44/58	0.79	7.7	0.20	1.29
NiO _{3S} 10 min	311	45/59	1.06	10.3	0.15	0.97
NiO _{3S} 20 min	306	46/59	3.98	38.8	0.04	0.26

loading.^[38,39] The lower availability of material in the 5 min. electrode has provide less OER sites, leading the overpotential increase.

Regarding the OER kinetics, the Tafel slopes are reported in Figure 4c. The plot shows the presence of two slopes. A lower slope ≈ 45 mV dec⁻¹, at the early stage of OER, and a higher one once the overpotential increases ≈ 60 mV dec⁻¹.

Focusing on the early stage OER kinetics, it is well known that in alkaline media the OH⁻ absorption on the electrocatalysts surface and the charge transfer is considered the rate determining step. Thus, a Tafel slope ≈ 45 mV dec⁻¹ agrees with this OER mechanism.^[40]

The increases of the slope with the overpotential, instead, is generally associated to the lower availability of adsorption sites slowing the kinetics.

We now want to focus on OER intrinsic activity. In Table 3, the values of TOF and mass activity calculated at a current density of 10 mA cm⁻² are reported. TOF was calculated extracting the number of moles from the catalyst mass derived from the Ni dose for each electrode.

The highest TOF obtained was for the NiO_{3S} 5 min of 0.20 s⁻¹. The NiO_{3S} 5 min electrode contains the lowest amount of material, thus lowest number of moles for the TOF calculation; however, it has a high overpotential (Figure 4). The TOF value of the NiO_{3S} 10 min is lower than NiO_{3S} 5 min; however, even possessing higher amount of catalyst, it reaches the desired current density at a lower overpotential. Thus, it gets a compromise of extrinsic and intrinsic catalytic activity. Once the catalyst loading increases, the TOF drastically decreases. This is what the NiO_{3S} 20 min shows, having the lowest overpotential. Moreover,

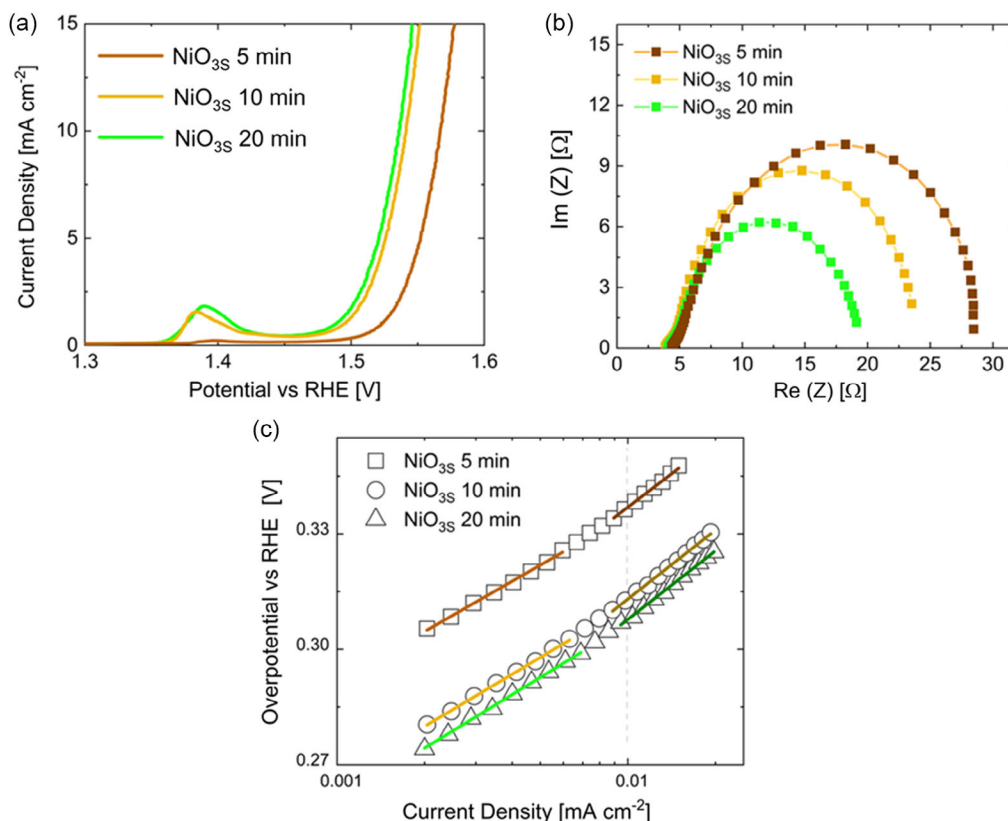


Figure 4. a) Linear sweep voltammetry (LSV) curves obtained for the electrodes dropped with the NPs PLAL obtained at 5, 10, and 20 min of ablation. b) Tafel slopes of the NiO_{3S} 5, 10, and 20 min. c) Electrochemical impedance spectroscopy (EIS) plot for the electrodes tested for oxygen evolution reaction (OER).

the Nyquist plots reported in Figure S3a, Supporting Information, show that the NiO_{3S} 20 min has the lower charge-transfer resistance (R_{CT}) probably due to a higher electrochemically active surface area consequence of the high amount of catalyst.^[41] However, even though having those high content of catalyst provides a low overpotential, this is not ensuring a significant intrinsic catalytic activity.

As one of the main goals, we aim is having a significant electrocatalytic activity with a small amount of electrocatalysts, the mass activity was evaluated. Mass activity values obtained at 10 mA cm⁻² are listed in Table 3. NiO_{3S} 5 min and NiO_{3S} 10 min have the highest mass activity values.

What emerges from the electrochemical results is that NiO_{3S} 10 min provides a balance between the extrinsic and intrinsic catalytic activity. Still having a highest mass activity, NiO_{3S} 5 min does not ensure enough current at low overpotential. The slow O₂ evolution and the high overpotential of the NiO_{3S} 5 min could be due to the scarcity of OER-accessible sites.

Another important aspect to study was the stability of the PLAL-based electrodes. **Figure 5** reports a chronoamperometry measurement performed at the NiO_{3S} 5 min electrode at 10 mA cm⁻² for 12 h in 1 M KOH. The variation of the overpotential after 12 h, compared to the initial value, was less than 1%. In the first hours of the measurements, a slightly decrease in the overpotential could be observed, maybe due to a further stabilization of the sample merged onto the electrolyte. Thereby,

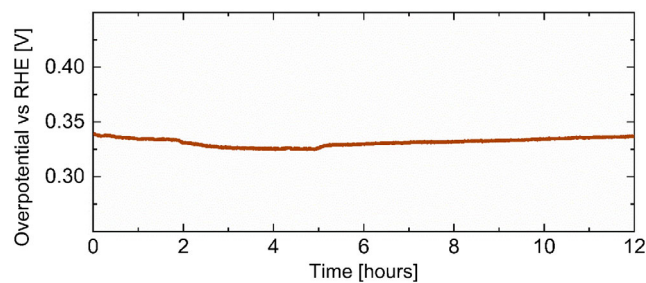


Figure 5. Chronoamperometry measurement performed at 10 mA cm⁻² for 12 h testing the stability of NiO_{3S} 5 min in 1 M KOH.

the electrode performance was not ruined by the extended activity, attesting a significant stability.

We now want to compare the obtained results with other Ni-based electrocatalyst tested in 1 M KOH reported in literature. The overpotential is reported at 10 mA cm⁻². In **Figure 6a**, bubble plot shows filled circles whose area indicates the catalyst loading (mg cm⁻²). Our results are indicated with blue circles. Others Ni- or NiO-based electrodes are instead represented by orange circles. The data represented in Figure 6 are reported in the ESI file in Table S3, Supporting Information.^[42–45] The optimized electrocatalyst are the ones which possess high mass activity and low overpotential. Indeed, those electrocatalyst positioned

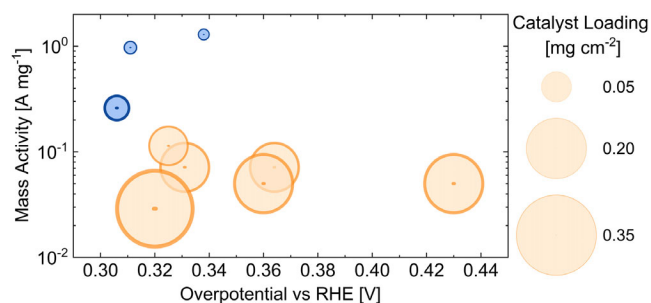


Figure 6. Bubble plot comparing Ni-based electrocatalyst tested in 1 M KOH reported in literature. The area of each circle is equal to the catalyst loading. Orange circles are referred to NiO-based electrocatalysts and blue ones are our results.^[42–45] The overpotential is reported at 10 mA cm⁻². The data represented in this plot are reported in Table S3, Supporting Information.

to the top-left part of this bubble plot are the ones with improved intrinsic activity and high OER performance.^[9] As shown, for the highest loaded PLAL-based electrode, the OER performance are the best compared to the others. Indeed, the 306 mV overpotential reached with $\approx 40 \mu\text{g}$ of Ni/NiO catalyst was a remarkable result in the framework of Ni/NiO-based electrocatalyst working in alkaline electrolyte. Nevertheless, even those electrodes loaded with the low-ablation time NP dispersions, still with a comparative overpotential at 10 mA cm⁻² toward the references, possess the best intrinsic activity per the OER.

Thus, the plot pointed out how the synthetic procedure impact the performances in terms of intrinsic behavior. In our case, PLAL method allowed to reach unprecedented mass activity at promising low overpotential thanks to a careful realization of electrode with a proper amount of Ni nanostructures.

4. Conclusions

In conclusion, we developed an efficient OER catalyst material by ablating a nickel target immersed in deionized water with a nano-second pulsed laser. The technique allowed us to obtain Ni/NiO NPs dispersions at different concentrations. The effectiveness of transfer methods of NPs onto GP substrate was studied through RBS measurements to establish the best way to get uniform NPs films. A Ni/NiO NPs/GP electrode was then prepared and tested to reach the best OER performance. An overpotential at 10 mA cm⁻² of 306 mV was achieved for 40 $\mu\text{g cm}^{-2}$ of catalyst, demonstrating the effectiveness of PLAL synthesis. Moreover, at the same current density, TOF of 0.20 s⁻¹ and mass activity of $\approx 1.3 \text{ A mg}^{-1}$ were reached by proper lowering the catalyst amount to 8 $\mu\text{g cm}^{-2}$. Then, Ni/NiO NPs produced by PLAL show OER performances comparable to critical raw materials such as Ir- and Ru-based ones, opening the route toward sustainable and efficient water-splitting for green hydrogen production. These data also encourage the use of PLAL as a green and efficient technique for electrocatalyst production.

Supporting Information

Supporting Information is available from the Wiley Online Library or from the author.

Acknowledgements

This work was supported by the project “Programma di ricerca di ateneo UNICT 2020–22 linea 2” of the University of Catania-Italy. This work has been partially funded by European Union (NextGeneration EU), through the MUR-PNRR project SAMOTHRACE (grant no. ECS00000022). The authors thank the Bio-nanotech Research and Innovation Tower (BRIT) laboratory of the University of Catania (grant no. PONA3_00136 financed by the MIUR) for the Smartlab diffractometer facility and Prof. G. Malandrino (uniCT) for kind availability related to XRD measurements; S. Tati, C. Percolla, and G. Pantè (CNR-IMM, Catania University, Italy) for technical support; Dott. L. Bruno for the electrochemical data analysis support; G.M. Di Mari for support in SEM images acquisition.

Open Access Funding provided by Università degli Studi di Catania within the CRUI-CARE Agreement.

Conflict of Interest

The authors declare no conflict of interest.

Data Availability Statement

The data that support the findings of this study are available from the corresponding author upon reasonable request.

Keywords

mass activity, NiO, oxygen evolution reaction, pulsed laser ablation in liquid, Rutherford backscattering spectrometry

Received: December 7, 2022

Revised: January 16, 2023

Published online:

- [1] U. Y. Qazi, *Energies* **2022**, *15*, 4741.
- [2] R. Javadi, *Catalysts* **2021**, *11*, 836.
- [3] M.-R. Gao, Y.-F. Xu, J. Jianga, S.-H. Yu, *Chem. Soc. Rev.* **2013**, *42*, 2986.
- [4] Y. Shia, B. Zhang, *Chem. Soc. Rev.* **2016**, *45*, 1529.
- [5] E. Fabbri, A. Habereeder, K. Waltar, R. Kötza, T. J. Schmidt, *Catal. Sci. Technol.* **2014**, *4*, 3800.
- [6] A. Carbone, S. C. Zignani, I. Gatto, S. Trocino, A. S. Aricò, *Int. J. Hydrog. Energy* **2020**, *45*, 9285.
- [7] Y. Matsumoto, E. Sato, *Mater. Chem. Phys.* **1986**, *14*, 397.
- [8] G. Li, L. Anderson, Y. Chen, M. Panb, P.-Y. A. Chuang, *Sustainable Energy Fuels* **2018**, *2*, 237.
- [9] J. Kibsgaard, I. Chorkendorff, *Nature Energy* **2019**, *4*, 430.
- [10] S. Anantharaj, S. Rao Ede, K. Sakthikumar, K. Karthick, S. Mishra, S. Kundu, *ACS Catal.* **2016**, *6*, 8069.
- [11] C. Hu, *Energy Environ. Sci.* **2019**, *12*, 2620.
- [12] F. M. Sapountzi, J. M. Gracia, C. J. (Kees-Jan) Weststrate, H. O. A. Fredriksson, J. W. (Hans) Niemantsverdriet, *Prog. Energy Combust. Sci.* **2017**, *58*, 1.
- [13] M. Schalenbach, A. R. Zeradhan, O. Kasian, S. Cherevko, K. J. J. Mayrhofer, *Int. J. Electrochem. Sci.* **2018**, *13*, 1173.
- [14] V. Amendola, D. Amans, Y. Ishikawa, N. Koshizaki, S. Scire, G. Compagnini, S. Reichenberger, S. Barcikowski, *Chem. Eur. J.* **2020**, *26*, 9206.
- [15] A. V. Shabalina, V. A. Svetlichnyi, S. A. Kulnich, *Curr. Opin. Green Sustainable Chem.* **2022**, *33*, 100566.

- [16] T. Begildayeva, D. Chinnadurai, S. J. Lee, Y. Yu, J. K. Song, M. Y. Choi, *J. Alloys Compd.* **2022**, *901*, 163446.
- [17] A. Shukla, S. C. Singh, C. S. Saraj, G. Verma, C. Guo, *Mater. Today Chem.* **2022**, *23*, 100691.
- [18] C. S. Saraj, S. C. Singh, A. Shukla, W. Yu, M. U. Fayyaz, C. Guo, *ChemElectroChem* **2021**, *8*, 209.
- [19] M. Gong, W. Zhou, M. C. Tsai, J. Zhou, M. Guan, M.-C. Lin, B. Zhang, Y. Hu, D.-Y. Wang, J. Yang, S. J. Pennycook, B.-J. Hwang, H. Dai, *Nat. Commun.* **2014**, *5*, 4695.
- [20] Y. Liu, C. Gao, Q. Li, H. Pang, *Chem. Eur. J.* **2019**, *25*, 2141.
- [21] M. Urso, F. Priolo, S. Mirabella, *Appl. Surf. Sci.* **2020**, *534*, 147585.
- [22] A. M. Mostafa, E. A. Mwafy, *Environ. Nanotechnol. Monit. Manage.* **2020**, *14*, 100382.
- [23] T. P. Mokoena, H. C. Swart, D. E. Motaung, *J. Alloys Compd.* **2019**, *805*, 267.
- [24] X. Zhuang, C. Tian, F. Luan, X. Wu, L. Chen, *RSC Adv.* **2016**, *6*, 92541.
- [25] S. C. Singh, H. Zeng, C. Guo, W. Cai, in *Nanomaterials: Processing and Characterization with Lasers*, Wiley-VCH, Weinheim **2012**, ch. 1, pp. 1–34.
- [26] M. Thompson, <https://www.genplot.com> (accessed: October 2021).
- [27] S. Anantharaj, P. E. Karthik, S. Noda, *Angew. Chem. Int. Ed.* **2021**, *60*, 23051.
- [28] S. Barcikowski, V. Amendola, G. Marzun, C. Rehbock, S. Reichenberger, D. Zhang, B. Gokce, *Handbook of Laser Synthesis & Processing of Colloids*, 2nd ed., Duisburg-Essen Publications Online **2019**, <https://doi.org/10.17185/dupublico/41087>.
- [29] M. A. Gondal, T. A. Saleh, Q. A. Drmosh, *Appl. Surf. Sci.* **2012**, *258*, 6982.
- [30] N. Lasemi, U. Pacher, C. Rentenberger, O. Bomati-Miguel, W. Kautek, *ChemPhysChem* **2017**, *18*, 1118.
- [31] R. Mahfouz, F. J. Cadete Santos Aires, A. Brenier, B. Jacquier, J. C. Bertolini, *Appl. Surf. Sci.* **2008**, *254*, 5181.
- [32] H. J. Jung, M. Y. Choi, *J. Phys. Chem. C* **2014**, *118*, 14647.
- [33] F. Mafuné, Jun-ya Kohno, Y. Takeda, T. Kondow, *J. Phys. Chem. B* **2003**, *107*, 4218.
- [34] L. Feldman, J. Mayer, *Fundamentals of Surface and Thin Film Analysis*, Elsevier Science Publishing Co, Inc., New York, NY **1986**.
- [35] P. Malinský, V. Hnatowicz, A. Macková, *Nucl. Instrum. Methods Phys. Res. B* **2016**, *371*, 101.
- [36] S. Anantharaj, S. Noda, *ChemElectroChem* **2020**, *7*, 2297.
- [37] S. Anantharaj, S. R. Ede, K. Karthick, S. Sam Sankar, K. Sangeetha, P. E. Karthick, S. Kundu, *Energy Environ. Sci.* **2018**, *11*, 744.
- [38] S. Anantharaj, S. Kundu, *ACS Energy Lett.* **2019**, *6*, 1260.
- [39] L. Bruno, M. Scuderi, F. Priolo, S. Mirabella, *Sustainable Energy Fuels* **2022**, *6*, 4498.
- [40] F. Davodi, *ACS Appl. Mater. Interfaces* **2018**, *10*, 31300.
- [41] H. Qayyum, C.-J. Tseng, T.-W. Huang, S.-Y. Chen, *Catalysts* **2016**, *6*, 180.
- [42] L.-A. Stern, L. Feng, F. Song, X. Hu, *Energy Environ. Sci.* **2015**, *8*, 2347.
- [43] X.-Y. Yu, Y. Feng, B. Guan, X. W. (David) Lou, U. Paik, *Energy Environ. Sci.* **2016**, *9*, 1246.
- [44] Y. Zhao, X. Jia, G. Chen, L. Shang, G. I. N. Waterhouse, L. Z. Wu, C. H. Tung, D. O'Hare, T. Zhang, *J. Am. Chem. Soc.* **2016**, *138*, 6517.
- [45] K. Fominykh, P. Chernev, I. Zaharieva, J. Sicklinger, G. Stefanic, M. Döblinger, A. Müller, A. Pokharel, S. Böcklein, C. Scheu, T. Bein, D. Fattakhova-Rohlfing, *ACS Nano* **2015**, *9*, 5180.